HHS Public Access

Author manuscript

J Am Chem Soc. Author manuscript; available in PMC 2016 December 09.

Published in final edited form as:

J Am Chem Soc. 2015 December 9; 137(48): 15330–15336. doi:10.1021/jacs.5b10675.

Mechanistic Insights into the H_2S-Mediated Reduction of Aryl Azides Commonly Used in H_2S Detection

Hillary A. Henthorn and **Michael D. Pluth**[*]

Department of Chemistry and Biochemistry, Institute of Molecular Biology, and Materials Science Institute, University of Oregon, Eugene, Oregon 97403, United States

Abstract

Hydrogen sulfide (H_2S) is an important biological mediator and has been at the center of a rapidly expanding field focused on understanding the biogenesis and action of H_2S as well as other sulfur-related species. Concomitant with this expansion has been the development of new chemical tools for H_2S research. The use of H_2S-selective fluorescent probes that function by H_2S-mediated reduction of fluorogenic aryl azides has emerged as one of the most common methods for H_2S detection. Despite this prevalence, the mechanism of this important reaction remains under-scrutinized. Here we present a combined experimental and computational investigation of this mechanism. We establish that HS^-, rather than diprotic H_2S, is the active species required for aryl azide reduction. The hydrosulfide anion functions as a one-electron reductant, resulting in the formation of polysulfide anions, such as HS_2^-, which were confirmed and trapped as organic polysulfides by benzyl chloride. The overall reaction is first-order in both azide and HS^- under the investigated experimental conditions with $\Delta S^{\ddagger}$ = –14(2) eu and $\Delta H^{\ddagger}$ = 13.8(5) kcal/mol in buffered aqueous solution. By using NBu_4SH as the sulfide source, we were able to observe a reaction intermediate (λ_{max} = 473 nm), which we attribute to formation of an anionic azidothiol intermediate. Our mechanistic investigations support that this intermediate is attacked by HS^- in the rate-limiting step of the reduction reaction. Complementing our experimental mechanistic investigations, we also performed DFT calculations at the B3LYP/6-31G(d,p), B3LYP/6-311++G(d,p), M06/TZVP, and M06/def2-TZVPD levels of theory applying the IEF-PCM water and MeCN solvation models, all of which support the experimentally determined reaction mechanism and provide cohesive mechanistic insights into H_2S-mediated aryl azide reduction.

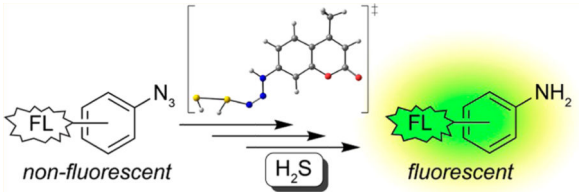

[*]**Corresponding Author**, pluth@uoregon.edu.

Supporting Information

The Supporting Information is available free of charge on the ACS Publications website at DOI: 10.1021/jacs.5b10675.

UV–vis spectra, Eyring plot, control experiments, computational data, and a list of references using azide reduction for H_2S sensing (PDF)

The authors declare no competing financial interest.

INTRODUCTION

Hydrogen sulfide (H_2S) has emerged as an important biological molecule of interest and joins nitric oxide (NO) and carbon monoxide (CO) as the third recognized gasotransmitter. Highlighting the importance of biological H_2S, endogenous sulfide plays critical roles in the cardiovascular, gastrointestinal, immune, and nervous systems. Enzymatic H_2S synthesis occurs primarily from cystathionine-β-synthase (CBS), cystathionine-γ-lyase (CSE), and 3-mercaptopyruvate sulfurtransferase (3-MST) working in concert with cysteine aminotransferase (CAT), although recent reports have also documented efficient H_2S synthesis from D-Cys with D-amino acid oxidase (DAO) and 3-MST. Because H_2S is a weak acid, about 80% of H_2S exists as monoanionic HS^- under physiological conditions. These different protonation states, along with the complex redox chemistry of sulfur, provide H_2S with a more complex reactivity profile than that of NO or CO, resulting in reactions of H_2S with both organic and inorganic targets. For example, the oxidative post-translational S-persulfidation of cysteine residues can enhance enzyme activity, and the reaction of H_2S with metalloprotein transition-metal centers may also contribute to key signaling pathways. Although many of the molecular mechanisms of action remain to be elucidated, H_2S is now known to be involved in a diverse array of important biochemical processes including vasorelaxation, neuronal long-term potentiation, insulin regulation, angiogenesis, and inflammation. Similarly, misregulation of endogenous H_2S concentrations is associated with various conditions including hypertension, Down syndrome, and diabetes.

Paralleling the discovery of new biological roles of H_2S has been the rapid expansion of chemical tools to study H_2S in biological contexts. Such advances have included the development of chemical methods for H_2S quantification, methods of H_2S delivery, and reaction-based tools for H_2S imaging. Fluorescent probe development has emerged as the most common imaging strategy and has relied on three main detection strategies, which include metal precipitation, nucleophilic attack, and reduction of azide or nitro groups. Of these methods, the H_2S-mediated reduction of azides (Figure 1) has emerged as the most common strategy for H_2S detection. In these systems, protection of a fluorogenic amine nitrogen as an azide renders the fluorophore nonemissive until the azide is reduced to the amine by H_2S. Highlighting the prevalence and impact of this sensing strategy, over 65 papers reporting azide-based H_2S probes have been published since the initial report of SF1 and SF2 in 2011. Despite this widespread use, the mechanism by which H_2S reduces aryl azides remains underinvestigated, and key questions related to this process remain. For example, does H_2S act as a one- or two-electron reductant? Is $H_2S(g)$ or HS^- the active sulfide species involved in the reduction? How many equivalents of H_2S are required for azide reduction? In addition to providing key insights into H_2S sensing, a functional understanding of how this reaction occurs would also provide valuable insights into the design of next-generation sensors. In view of this critical need, here we report experimental and computational investigations that provide new insights into the mechanism of H_2S-mediated azide reduction.

RESULTS AND DISCUSSION

On the basis of the high nucleophilicity of HS^- as well as its prevalence under physiological conditions, it is likely that HS^- rather than H_2S is the active species required for azide reduction. Drawing parallels to analogous reactions of azides with other nucleophilic reductants, such as phosphines in the Staudinger reaction, in which the terminal nitrogen is the site of nucleophilic attack, our expectation is that the sulfide-mediated reduction of aryl azides proceeds through initial nucleophilic attack on the electrophilic azide. After this initial attack to form an anionic azidothiol intermediate, we envisioned two possible mechanisms to generate the arylamine product (Scheme 1). The first mechanism proceeds through an intramolecular reaction in which proton transfer generates a terminal thiolate, which subsequently attacks the azide through either a four-membered triazathiocyclobutyl or three-membered diazathiocyclopropyl transition state to release N_2, S^0, and the arylamine product (mechanism I). In this scenario, H_2S would act as a two-electron reductant, and a large, negative value of the entropy of activation ($\Delta S^{\ddagger}$) would be expected. By contrast to this intramolecular mechanism, the anionic azidothiol intermediate could be attacked by a second equivalent of HS^-. In this scenario, protonation of the anionic azidothiol to generate a neutral azidothiol intermediate could enhance its electrophilicity, thus resulting in further activation for attack by the second equivalent of HS^- to release N_2, HS_2^-, and the arylamine product (mechanism II). In this mechanism, H_2S would act as a one-electron reductant, and a moderately negative $\Delta S^{\ddagger}$, corresponding to a bimolecular reaction, would be expected.

Kinetic Studies of the H_2S-Mediated Reduction of C7-Az

To investigate the mechanism of sulfide-mediated azide reduction, we chose to use the previously reported 4-methyl-7-azidocoumarin (C7-Az) (Figure 1) as a model system because of its ease of synthesis and amenable spectroscopic properties. Treatment of aqueous buffered solutions of C7-Az with excess sodium hydrosulfide (NaSH) under pseudo-first-order conditions resulted in a decrease in the C7-Az absorbance (λ_{max} = 326 nm) and concomitant formation of C7-NH_2 (λ_{max} = 343 nm) with a well-anchored isosbestic point at 334 nm (Figure 2a). Under our experimental conditions, conversion to the amine is complete within 60 min, making the reaction amenable for kinetic investigations. We also verified that the fluorescence turn-on profile of C7-Az matched the UV–vis data. Plots of the absorbances at 326 and 343 nm versus time (Figure 2b) both fit the first-order rate equation (Figure S1), and such fits were used to obtain pseudo first-order rate constants (k_{obs}) for subsequent experiments unless otherwise specified. Although sulfide-mediated azide reduction is likely a multistep process, no intermediates were observed by UV–vis spectroscopy.

Reaction Order and Activation Parameters

To determine the reaction orders with respect to [C7-Az] and [NaSH], we measured the rate of the reaction as a function of the reactant concentrations at constant pH and temperature. Working under pseudo first-order conditions in sulfide, varying [NaSH] allowed for determination of the [NaSH] order from a plot of log(k_{obs}) versus log([NaSH]). This plot provided a linear relationship with a slope of 0.99, suggesting a first-order rate dependence on [NaSH] (Figures 3a and S3). To determine the reaction order with respect to C7-Az,

kinetic data were collected at constant pH, [NaSH], and temperature. To aid experimental measurement of k_{obs} for these experiments, we monitored initial rates because of the small changes in the absorbance of C7-Az and C7-NH_2 during the course of the reaction. The resultant plot of log(k_{obs}) versus log([C7-Az]) also provided a linear plot with a slope of 0.94, which is also consistent with a first-order rate dependence on [C7-Az] (Figures 3b and S3). Supplementing the reaction order data, we also measured the rates of the reduction from 283–308 K under pseudo-first-order conditions in [NaSH] and calculated the second-order rate constants from the resultant k_{obs} data, which ranged from 0.12 M^{-1} s^{-1} at 283 K to 0.95 M^{-1} s^{-1} at 308 K. Eyring analysis of the resultant second-order rate data revealed $\Delta H^{\ddagger}$ = 13.8(5) kcal/mol and $\Delta S^{\ddagger}$ = –14(2) eu (Figure S2). The moderately negative $\Delta S^{\ddagger}$ supports a rate-limiting step that proceeds through a bimolecular transition state rather than the highly strained intramolecular transition state associated with mechanism I.

Observation of Reaction Intermediates

To better isolate and differentiate the impacts of the H_2S and HS^- protonation states, we also investigated the reduction reaction in organic solution. Additionally, on the basis of the mechanisms proposed in Scheme 1, we envisioned that the use of an aprotic solvent could facilitate the observation of the proposed anionic intermediates. We chose to use MeCN as the solvent because of its high dielectric constant and aprotic nature. In support of our hypothesis that HS^-, rather than H_2S(g), is the active sulfide source in the reduction reaction, treatment of C7-Az with excess H_2S(g) failed to produce any reaction. By contrast, addition of NBu_4SH, which is a source of HS^- that is soluble in organic solvents, resulted in the immediate formation of an orange intermediate with an absorbance at 473 nm. During the course of the reaction, the absorbance of this highly colored intermediate slowly decayed to an absorbance corresponding to the C7-NH_2 product (Figure 4a). A plot of the absorbance values for C7-NH_2 at 334 nm and the intermediate at 473 nm fit cleanly to a first-order rate equation with nearly identical k_{obs} values of 0.204 and 0.197 s^{-1}, respectively (Figure 4b). These rate data support that rate-limiting decomposition of the observed intermediate leads to C7-NH_2 product formation. As control experiments, we confirmed that the absorbance at 473 nm does not correspond to other possible products formed during the course of the reaction, including hydropolysulfide anions (HS_x^-), trisulfide radical ion ($S_3^{\bullet -}$), and deprotonated amine (C7-NH^-) (Figures S5 and S7). In further support of the anionic structure of the intermediate, addition of an excess of H_2O abolished the 473 nm absorbance and resulted in partial product formation, suggesting that protonation of the azidothiolate intermediate is required for subsequent sulfide attack (Figure S6). Using fluorescence spectroscopy, we also confirmed that the C7-Az fluorescence response is due to C7-NH_2 formation rather than formation of the intermediate.

In addition to providing a solvent in which an intermediate could be observed, the use of aprotic MeCN in combination with NBu_4SH allowed for titration of C7-Az to determine the reaction stoichiometry of HS^- required to complete the reduction. These experiments demonstrated that complete conversion of the azide starting material to the amine product did not occur until 2 equiv of HS^- had been added (Figure 5), which suggests not only that HS^- functions as a one-electron reductant but also that 2 equiv of HS^- is required for the

reaction. The requirement of 2 equiv of HS^- supports mechanism II (Scheme 1), in which HS^- acts as a one electron reductant.

To gain further insights into the identity of the oxidized sulfur products formed during azide reduction, we treated C7-Az with 3 equiv of NBu_4SH in MeCN and trapped the sulfur species present at the end of the reaction with benzyl chloride (BnCl). On the basis of the proposed reaction stoichiometry, we expected to observe 1 equiv of unreacted HS^- and 1 equiv of oxidized sulfur products. Consistent with this hypothesis, we observed 1 equiv of Bn_2S (3.67 ppm) and Bn_2S_2 (3.72 ppm) as well as a small peak corresponding to higher-order benzyl polysulfides (4.45 ppm) (Figure 6). Importantly, the formation of Bn_2S_2 confirmed that HS_2^- was formed during the azide reduction reaction.

Proposed Mechanism

Taken together, the experimental results detailed above support mechanism II, which is outlined in greater detail in Scheme 2. The first step of the reaction proceeds by reversible nucleophilic attack of HS^- on the terminal azide nitrogen of C7-Az (**1**), which is the most electrophilic nitrogen of the azide. Nucleophilic attack on the terminal nitrogen has precedent in the Staudinger reaction as well as the addition of carbon-based nucleophiles to azides. This initial nucleophilic attack generates anionic azidothiol intermediate **2**, which we assign to the absorbance at 473 nm observed in MeCN on the basis of the experiments described above as well as qualitative time-dependent density functional theory (TD-DFT) calculations that support a bathochromic shift upon formation of the anionic azidothiol intermediate (Figure S9). Although anionic azidothiol **2** could be attacked directly by HS^-, it is more plausible that **2** is transiently protonated to generate neutral **3**, which would be significantly more electrophilic. Subsequent attack on **3** by a second equivalent of HS^- then generates deprotonated amine **4**, N_2, and H_2S_2, after which proton transfer, likely mediated by the solvent, results in the formation of C7-NH_2 (**5**). We note that anion **4** is a significantly stronger base than intermediate **2** or HS_2^- and should undergo facile proton transfer to generate **5**. This proposed mechanism is consistent with the observed first-order dependence of the reaction rate on HS^- and azide as well as the moderately negative $\Delta S^{\ddagger}$ for the reaction.

Rate Law Analysis

On the basis of the mechanism outlined in Scheme 2, the overall rate law for product formation can be derived from the reaction scheme shown in eq 1, in which 2 equiv of HS^- and 1 equiv of aryl azide are involved in the reaction:

$$\mathbf{1} + \mathbf{HS^-} \underset{k_{-1}}{\overset{k_1}{\rightleftarrows}} \mathbf{2} \underset{k_{-2}}{\overset{k_2[H^+]}{\rightleftarrows}} \mathbf{3} \xrightarrow{k_3[\mathbf{HS^-}]} \text{product} \quad (1)$$

To simplify this reaction scheme, we note that conversion of **1** to **3** requires the net addition of H_2S(g) to **1**, thus allowing for simplification of eq 1 to obtain eq 2:

$$\mathbf{1}+\mathrm{H_2S} \underset{\mathbf{k'_{-1}}}{\overset{\mathbf{k'_1}}{\rightleftarrows}} \mathbf{3} \xrightarrow{\mathbf{k_3[HS^-]}} \text{product} \quad (2)$$

Under this scenario, anionic azidothiol intermediate **3** is formed through a rapid pre-equilibrium before the rate-limiting attack by HS^-, thus leading to the simplified steady-state rate law shown in eq 3:

$$\text{rate}=k_3\left[HS^-\right]\left(\frac{k'_1\left[ArN_3\right]\left[\mathrm{H_2S}\right]}{k_3\left[HS^-\right]+k'_{-1}}\right) \quad (3)$$

In the limiting case in which $k_2\left[HS^-\right] \ll k'_{-1}$, which would result at low sulfide concentrations or if the unimolecular disassociation of azidothiol intermediate **3** is very fast, the rate law would condense to the form shown in eq 4:

$$\text{rate}=\frac{k'_1}{k'_{-1}}k_3\left[ArN_3\right]\left[HS^-\right]\left[\mathrm{H_2S}\right] \quad (4)$$

However, under conditions in which $k_3\left[HS^-\right] \gg k'_{-1}$, which would occur at higher [HS^-], the rate law condenses to the form shown in eq 5:

$$\text{rate}=k'_1\left[ArN_3\right]\left[\mathrm{H_2S}\right] \quad (5)$$

Under the experimental reaction conditions, we observe a first-order dependence of the rate on both [ArN_3] and [HS^-], which would be expected when [HS^-] is in excess and is consistent with eq 5. Our attempts to shift the reaction to the other regime, in which a second-order dependence on sulfide is observed, including the use of C7-Az as the flooding substrate, maintained a first-order sulfide dependence, suggesting that we are experimentally unable to access the other limiting condition. However, when taken in combination with the reaction stoichiometry data and trapping of the HS_2^- reaction product (vide supra) and DFT reaction coordinate calculations (vide infra), these kinetic data support the proposed mechanism for sulfide-mediated aryl azide reduction.

DFT Calculations

To provide added insights into the feasibility and energetics of the mechanism proposed in Scheme 2, we also conducted a full conformational search of each reactant, product, and intermediate and located each transition state using Gaussian 09 at the B3LYP/6-31G(d,p), B3LYP/6-311++G(d,p), M06/TZVP, and M06/def2-TZVPD levels of theory applying the IEF-PCM water and MeCN solvation models. The calculated potential energy surfaces (PESs) obtained at the B3LYP/6-311++G(d,p) and M06/def2-TZVPD levels of theory with the H_2O solvation model are shown in Figure 7. Starting from C7-Az (**1**), the transition state

of the first nucleophilic attack (**TS_{12}**) was located with a calculated energy barrier of 9.1 kcal/mol, and from **TS_{12}** the reaction proceeds to generate anionic azidothiol intermediate **2** with an overall endothermicity of 4.4 kcal/mol. Attempts to locate transition state structures derived from the attack of HS^- on anionic **2** were unsuccessful, whereas protonation of **2** to form neutral azidothiol intermediate **3** proceeds with a modest enthalpic penalty of 2.6 kcal/mol. Subsequent nucleophilic attack by HS^- on **3** proceeds through transition state **TS_{34}**, which has a local energy barrier of 9.2 kcal/mol to generate the deprotonated amine which is then protonated to generate the highly thermodynamically favored C7-NH_2 product (–59.5 kcal/mol). This second nucleophilic attack proceeds with the HS^- attacking the electrophilic sulfhydryl group of azidothiol intermediate **3** and is also consistent with the high homophilicity of sulfur. The calculated PES indicates that the second nucleophilic attack is the rate-determining step with an overall activation enthalpy of 16.2 kcal/mol, which is in good agreement with the experimentally measured $\Delta H^{\ddagger}$ of 13.8(5) kcal/mol. No significant difference in the relative energies was observed when comparing the results between the DFT functionals and basis sets, highlighting the robust energy landscape derived from these computation studies. Although one would expect diffuse functions and dispersion forces to play an important role in this transformation, they have little impact on the thermochemistry of this PES (Figure S8). Significant efforts to locate transition state structures corresponding to the intramolecular 3- or 4-membered transitions states required in mechanism I were unsuccessful.

Mechanistic Insights

The experimental and computational investigations outlined above provide a cohesive mechanism for sulfide-mediated reduction of aryl azides. A number of key points are highlighted below. First, the mechanistic studies establish that HS^-, rather than H_2S, is the active species responsible for sulfide-mediated azide reduction. Because HS^- is the dominant species under physiological conditions, these results highlight that the azide reduction method reports on the most prevalent form of available sulfide. Additionally, the initial addition of HS^- to the azide is reversible, suggesting that generation of the important azidothiol intermediate may be difficult under conditions where the sulfide concentrations are very low. It is possible that other sulfhydryl-containing biomolecules, such as glutathione, may participate in the reaction after the initial attack by the more nucleophilic hydrosulfide anion. Furthermore, the mechanistic insights suggest that protonation of the azidothiolate intermediate is an important step in the reaction. One would expect that addition of functional groups that could make this intermediate more basic and favor protonation would help to drive the reaction, thus facilitating nucleophilic attack in the subsequent and rate-limiting step. Additionally, these mechanistic studies show that HS^- is consumed during each reduction of an aryl azide, highlighting that such sensing methods perturb the sulfide levels and the redox state of the system. On the basis of the growing importance of the reduction-labile sulfane sulfur pool, such reaction-based detection methods may inadvertently disturb the distribution of sulfide between the bound and free pools, thus opening new questions related to how H_2S sensors impact redox homeostasis. With the absence of reversible H_2S sensing mechanisms that operate under physiological conditions, such perturbations remain a reality of reaction-based sensors and need to be considered for biological inquiries in which irreversible reaction-based reporters are used.

CONCLUSIONS

Our mechanistic investigations into the sulfide-mediated reduction of aryl azides have revealed that this reaction is first-order with respect to C7-Az and NaSH under our experimental conditions and proceeds with activation parameters consistent with a biomolecular mechanism ($\Delta S^{\ddagger}$ = –14(2) eu) with a moderate enthalpic barrier ($\Delta H^{\ddagger}$ = 13.8(5) kcal/mol). Reactions of C7-Az with NBu_4SH in MeCN allowed for the observation of an absorbance that we attribute to the anionic azidothiol intermediate, and HS^- titrations in this system established that 2 equiv of HS^- is required for complete reduction, which is consistent with sulfide acting as a one-electron reductant. Computational studies support the experimental observations and indicate that the second attack of sulfide is the rate-determining-step of the reduction, and the calculated activation energy (16.2 kcal/mol) is in good agreement with the experimental enthalpy of activation (13.8(5) kcal/mol). Taken together, the results of these mechanistic studies provide new insights into the individual steps required for H_2S-mediated azide reduction and may be useful in the refinement of this important sensing strategy for H_2S.

EXPERIMENTAL DETAILS

Materials and Methods

All manipulations were performed under an inert atmosphere using standard Schlenk techniques or an Innovative Atmospheres N_2-filled glovebox with O_2 levels less than 1.0 ppm. Anhydrous and air-free MeCN was obtained from a Pure Process Technologies solvent purification system. Deuterated solvents were dried by distillation over the appropriate drying agent and deoxygenated by three freeze–pump–thaw cycles. Tetrabutylammonium hydrosulfide (NBu_4SH) and C7-Az were prepared as described in the literature. Anhydrous sodium hydrogen sulfide (NaSH) was purchased from Strem Chemicals and handled under nitrogen. Piperazine-*N*,*N*′-bis(2-ethanesulfonic acid) (PIPES) and potassium chloride (99.999%), both obtained from Aldrich, were used to make buffered solutions (50 mM PIPES, 100 mM KCl, pH 7.4) with Millipore water. Buffered solutions were degassed by vigorous sparging with N_2 and stored in an inert atmosphere glovebox. Stock solutions of C7-Az were prepared in MeCN or dimethyl sulfoxide. Gas-tight Hamilton syringes were used for solution transfers outside of the glovebox.

Spectroscopic Methods

UV–vis measurements were performed on an Agilent Cary 100 UV–vis spectrophotometer equipped with a QNW dual-cuvette temperature controller at 25.00 ± 0.05 °C. All of the cuvette-based spectroscopic measurements were made under anaerobic conditions with solutions prepared under an inert atmosphere in 1.0 cm path length septum-sealed cuvettes obtained from Starna Scientific and were repeated at least in duplicate. NMR spectra were acquired on a Bruker Avance-III-HD 600 spectrometer with a Prodigy multinuclear broadband cryoprobe at 25.0 °C.

Computational Details

Calculations were performed using the Gaussian 09 software package. Chemcraft was used to analyze the results and generate graphical representations. Conformational searches were conducted at the B3LYP/6-311++G(d,p), M06/TZVP, and M06/def2-TZVPD levels of theory applying the IEF-PCM water and MeCN solvation models by exploring reasonable input dihedral angles. Frequency calculations were performed on each located stationary point to confirm that it was either a local minimum or a saddle point. Relative energies were calculated using the zero-point-energy-corrected electronic energies obtained in the frequency calculations.

General Conditions for UV–Vis Experiments

In a septum-sealed cuvette, 2.970 mL of a 20 μM stock solution of C7-Az in either MeCN or buffered water was treated with 30 μL of 200 mM HS^- stock solution. The UV–vis spectra were monitored as a function of time, and the C7-NH_2 absorbance (343 nm) was used to measure the observed rate constants.

General Conditions for NMR Experiments

A septum-sealed NMR tube was charged with C7-Az (12 mM in 0.5 mL MeCN-d_3) under a nitrogen atmosphere, and 6.6 μL of triethylamine was added. A 50 μL aliquot of a MeCN-d_3 solution containing 240 mM NBu_4SH was added. The azide was completely reduced upon sulfide addition, and BnCl (5.5 μL) was added to trap the generated HS_2^-. Authentic Bn_2S_2 was subsequently added to confirm the identity of the singlet at 3.72 ppm. All additions were performed using Hamilton syringes.

Supplementary Material

Refer to Web version on PubMed Central for supplementary material.

ACKNOWLEDGMENTS

This work was supported by NIH Grant 1R01GM113030 and the Sloan Foundation. The NMR facilities at the UO are supported by the NSF/ARRA (CHE-0923589), and the computational infrastructure is supported by the OCI (OCI-0960354).

REFERENCES

1. Wang R. Physiol. Rev. 2012; 92:791–896. [PubMed: 22535897]
2. We will use “H_2S” to denote the totality of the sulfide pool, which includes H_2S, HS^-, and S^{2-}. When we are clearly defining one protonation state, we will use H_2S(g) or HS^- for added clarity.
3. Abe K, Kimura HJ. Neurosci. 1996; 16:1066–1071.
4. Hosoki R, Matsuki N, Kimura H. Biochem. Biophys. Res. Commun. 1997; 237:527–531. [PubMed: 9299397]
5. Shibuya N, Tanaka M, Yoshida M, Ogasawara Y, Togawa T, Ishii K, Kimura H. Antioxid. Redox Signaling. 2009; 11:703–714.
6. Mustafa AK, Gadalla MM, Sen N, Kim S, Mu WT, Gazi SK, Barrow RK, Yang GD, Wang R, Snyder SH. Sci. Signaling. 2009; 2:ra72.

7. a Dorman DC, Moulin FJ-M, McManus BE, Mahle KC, James RA, Struve MF. Toxicol. Sci. 2002; 65:18–25. [PubMed: 11752681] b Collman JP, Ghosh S, Dey A, Decreau RA. Proc. Natl. Acad. Sci. U. S. A. 2009; 106:22090–22095. [PubMed: 20007376]
8. a Yang G, Yang W, Wu L, Wang RJ. Biol. Chem. 2007; 282:16567–16576.b Yang W, Yang GD, Jia XM, Wu LY, Wang R. J. Physiol. 2005; 569:519–531. [PubMed: 16179362]
9. a Papapetropoulos A, Pyriochou A, Altaany Z, Yang GD, Marazioti A, Zhou ZM, Jeschke MG, Branski LK, Herndon DN, Wang R, Szabo C. Proc. Natl. Acad. Sci. U. S. A. 2009; 106:21972–21977. [PubMed: 19955410] b Cai WJ, Wang MJ, Moore PK, Jin HM, Yao T, Zhu YC. Cardiovasc. Res. 2007; 76:29–40. [PubMed: 17631873]
10. Kaneko Y, Kimura Y, Kimura H, Niki I. Diabetes. 2006; 55:1391–1397. [PubMed: 16644696]
11. Yang G, Wu L, Jiang B, Yang W, Qi J, Cao K, Meng Q, Mustafa AK, Mu W, Zhang S, Snyder SH, Wang R. Science. 2008; 322:587–590. [PubMed: 18948540]
12. Kamoun P, Belardinelli MC, Chabli A, Lallouchi K, Chadefaux-Vekemans B. Am. J. Med. Genet. Part A. 2003; 116A:310–311. [PubMed: 12503113]
13. Wu LY, Yang W, Jia XM, Yang GD, Duridanova D, Cao K, Wang R. Lab. Invest. 2009; 89:59–67. [PubMed: 19002107]
14. a Wintner EA, Deckwerth TL, Langston W, Bengtsson A, Leviten D, Hill P, Insko MA, Dumpit R, VandenEkart E, Toombs CF, Szabo C. Br. J. Pharmacol. 2010; 160:941–957. [PubMed: 20590590] b Shen X, Pattillo CB, Pardue S, Bir SC, Wang R, Kevil CG. Free Radical Biol. Med. 2011; 50:1021–1031. [PubMed: 21276849] c Shen X, Peter EA, Bir S, Wang R, Kevil CG. Free Radical Biol. Med. 2012; 52:2276–2283. [PubMed: 22561703] c Montoya LA, Pearce TF, Hansen RJ, Zakharov LN, Pluth MD. J. Org. Chem. 2013; 78:6550–6557. [PubMed: 23735055] e Montoya LA, Shen X, McDermott JJ, Kevil CG, Pluth MD. Chem. Sci. 2015; 6:294–300. [PubMed: 25632344]
15. a Benavides GA, Squadrito GL, Mills RW, Patel HD, Isbell TS, Patel RP, Darley-Usmar VM, Doeller JE, Kraus DW. Proc. Natl. Acad. Sci. U. S. A. 2007; 104:17977–17982. [PubMed: 17951430] b Song ZJ, Ng MY, Lee Z-W, Dai W, Hagen T, Moore PK, Huang D, Deng L-W, Tan C-H. MedChemComm. 2014; 5:557–570.c Wallace JL, Wang R. Nat. Rev. Drug Discovery. 2015; 14:329–345. [PubMed: 25849904] c Li L, Whiteman M, Guan YY, Neo KL, Cheng Y, Lee SW, Zhao Y, Baskar R, Tan CH, Moore PK. Circulation. 2008; 117:2351–2360. [PubMed: 18443240] e Zhao Y, Wang H, Xian M. J. Am. Chem. Soc. 2011; 133:15–17. [PubMed: 21142018] f Artaud I, Galardon E. ChemBioChem. 2014; 15:2361–2364. [PubMed: 25205314] g Le Trionnaire S, Perry A, Szczesny B, Szabo C, Winyard PG, Whatmore JL, Wood ME, Whiteman M. MedChemComm. 2014; 5:728–736.
16. Sasakura K, Hanaoka K, Shibuya N, Mikami Y, Kimura Y, Komatsu T, Ueno T, Terai T, Kimura H, Nagano T. J. Am. Chem. Soc. 2011; 133:18003–18005. [PubMed: 21999237]
17. a Liu CR, Pan J, Li S, Zhao Y, Wu LY, Berkman CE, Whorton AR, Xian M. Angew. Chem., Int. Ed. 2011; 50:10327–10329.b Qian Y, Karpus J, Kabil O, Zhang S-Y, Zhu H-L, Banerjee R, Zhao J, He C. Nat. Commun. 2011; 2:495. [PubMed: 21988911] c Chen YC, Zhu CC, Yang ZH, Chen JJ, He YF, Jiao Y, He WJ, Qiu L, Cen JJ, Guo ZJ. Angew. Chem., Int. Ed. 2013; 52:1688–1691.
18. See the Supporting Information for a list of citations using H_2S-mediated azide reduction as a sensing strategy.
19. a Gololobov YG, Zhmurova IN, Kasukhin LF. Tetrahedron. 1981; 37:437–472.b Gololobov YG, Kasukhin LF. Tetrahedron. 1992; 48:1353–1406.c Leffler JE, Temple RD. J. Am. Chem. Soc. 1967; 89:5235–5246.c Leffler JE, Tsuno Y. J. Org. Chem. 1963; 28:902–906.e Fortman GC, Captain B, Hoff CD. Inorg. Chem. 2009; 48:1808–1810. [PubMed: 19235943]
20. Chen B, Li W, Lv C, Zhao M, Jin H, Jin H, Du J, Zhang L, Tang X. Analyst. 2013; 138:946–951. [PubMed: 23243655]
21. Eyring analysis of the pseudo-first-order rate data afforded $\Delta H^{\ddagger} = 13.8(5)$ kcal/mol and $\Delta S^{\ddagger} = -26(2)$ eu, which is consistent with the change in standard-state entropy.
22. Brase S, Gil C, Knepper K, Zimmermann V. Angew. Chem., Int. Ed. 2005; 44:5188–5240.
23. For simplicity and to maintain atomic balance in the PES, we assumed that this protonation proceeded from H_2S.

24. a Thorson MK, Majtan T, Kraus JP, Barrios AM. Angew. Chem., Int. Ed. 2013; 52:4641–4644.b Hartle MD, Meininger DJ, Zakharov LN, Tonzetich ZJ, Pluth MD. Dalton. Trans. 2015; 44:19782–19785. [PubMed: 26536835]

25. Frisch, MJ.; Trucks, GW.; Schlegel, HB.; Scuseria, GE.; Robb, MA.; Cheeseman, JR.; Scalmani, G.; Barone, V.; Mennucci, B.; Petersson, GA.; Nakatsuji, H.; Caricato, M.; Li, X.; Hratchian, HP.; Izmaylov, AF.; Bloino, J.; Zheng, G.; Sonnenberg, JL.; Hada, M.; Ehara, M.; Toyota, K.; Fukuda, R.; Hasegawa, J.; Ishida, M.; Nakajima, T.; Honda, Y.; Kitao, O.; Nakai, H.; Vreven, T.; Montgomery, JA., Jr.; Peralta, JE.; Ogliaro, F.; Bearpark, M.; Heyd, JJ.; Brothers, E.; Kudin, KN.; Staroverov, VN.; Kobayashi, R.; Normand, J.; Raghavachari, K.; Rendell, A.; Burant, JC.; Iyengar, SS.; Tomasi, J.; Cossi, M.; Rega, N.; Millam, JM.; Klene, M.; Knox, JE.; Cross, JB.; Bakken, V.; Adamo, C.; Jaramillo, J.; Gomperts, R.; Stratmann, RE.; Yazyev, O.; Austin, AJ.; Cammi, R.; Pomelli, C.; Ochterski, JW.; Martin, RL.; Morokuma, K.; Zakrzewski, VG.; Voth, GA.; Salvador, P.; Dannenberg, JJ.; Dapprich, S.; Daniels, AD.; Farkas, Ö.; Foresman, JB.; Ortiz, JV.; Cioslowski, J.; Fox, DJ. Gaussian 09, revision C.01. Gaussian, Inc.; Wallingford, CT: 2009.

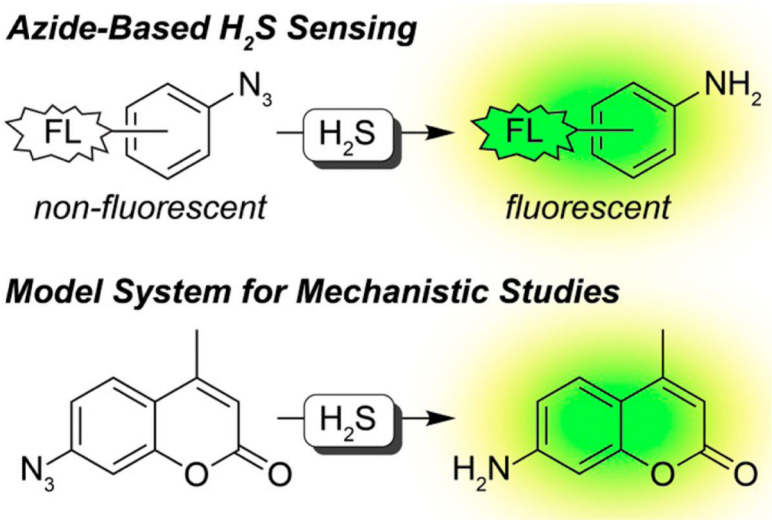

Figure 1.

(top) Example of H_2S-mediated azide reduction with a fluorescent turn-on response. (bottom) Model azide system used here for mechanistic studies.

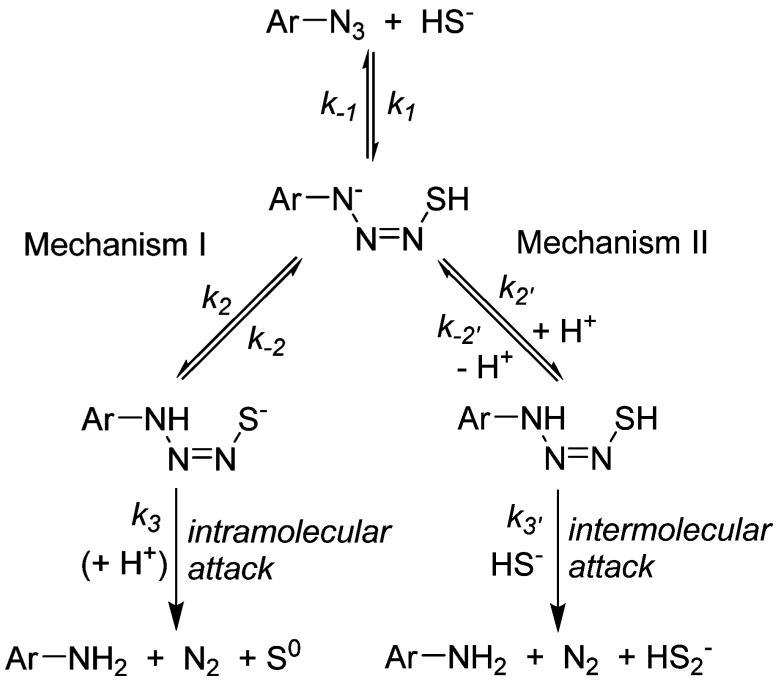

Scheme 1.

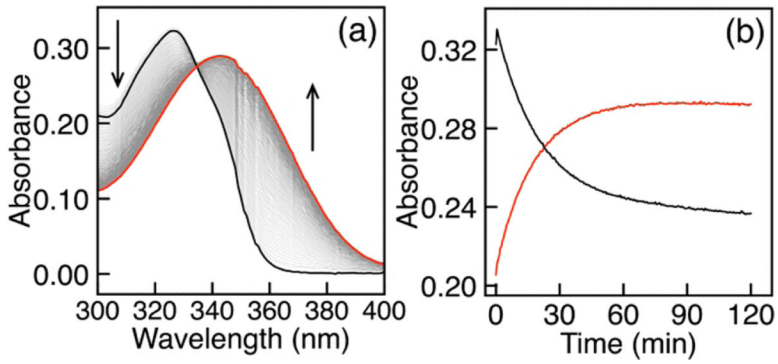

Figure 2.

(a) UV–vis spectra and (b) time course data for the reaction of C7-Az (black) with NaSH to form C7-NH_2 (red) under pseudo-first-order conditions (20 μM probe, 2.0 mM NaSH, 50 mM PIPES, 100 mM KCl, pH 7.4, 25 °C).

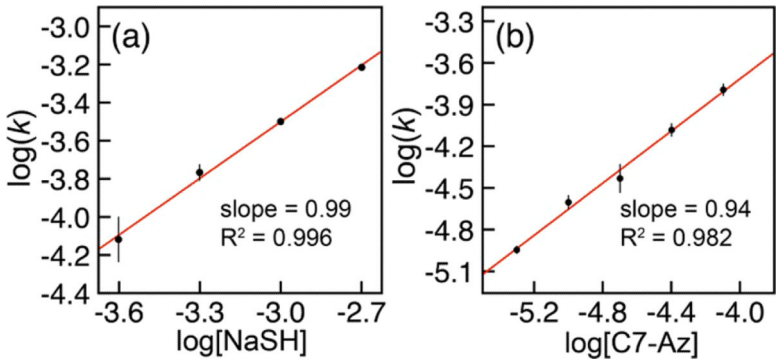

Figure 3.

(a) Plot of log(k_{obs}) vs log([NaSH]) for the reactions of 0.25–2.00 mM NaSH with 20 μM C7-Az. (b) Plot of log(k_{obs}) vs log([C7-Az]) for the reactions of 2.00 mM NaSH with 5–80 μM C7-Az. Standard conditions: 50 mM PIPES, 100 mM KCl, pH 7.4, 25 °C. Each measurement was repeated at least in triplicate.

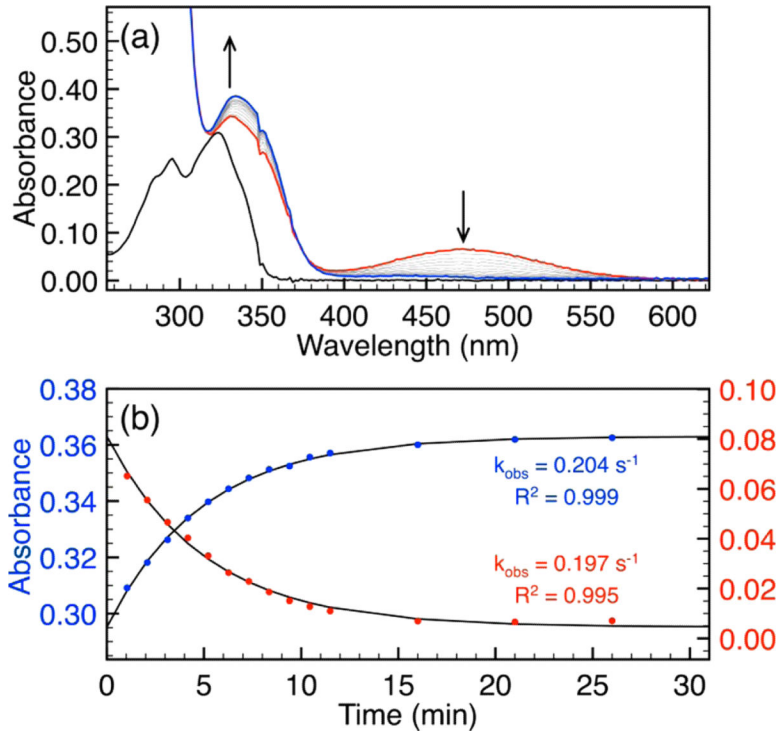

Figure 4.

Reaction of C7-Az with excess NBu_4SH (20 μM C7-Az, 2.0 mM NBu_4SH, MeCN): (a) full spectra overlay and (b) time courses at 334 (blue) and 473 (red) nm.

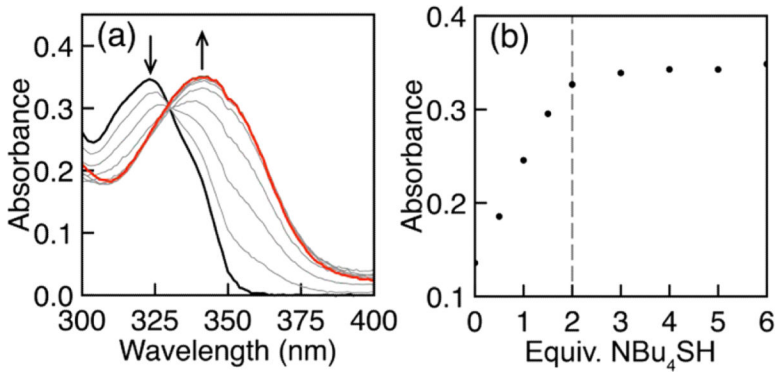

Figure 5.

(a) UV–vis titration showing the reduction of C7-Az (20 μM in MeCN) to C7-NH_2 (red) by NBu_4SH. (b) Monitoring the absorbance of the C7-NH_2 product as a function of NBu_4SH establishes that 2 equiv of HS^- are required for azide reduction.

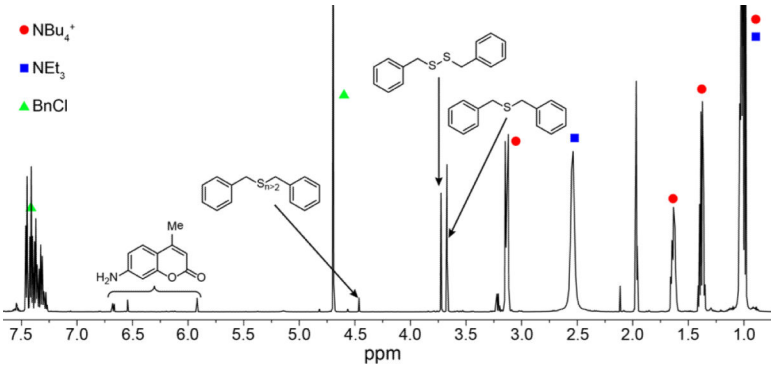

Figure 6.

^{1}H NMR spectrum (600 MHz) of the products formed during the reduction of C7-Az (12 mM) with NBu_4SH (36 mM, 3 equiv) in CD_3CN. Polysulfide anions formed during the reaction were trapped by addition of BnCl (12 equiv) and NEt_3 (12 equiv) after azide reduction was complete. The observation of Bn_2S_2 and higher-order organic polysulfides supports the formation of HS_x^- during the azide reduction process.

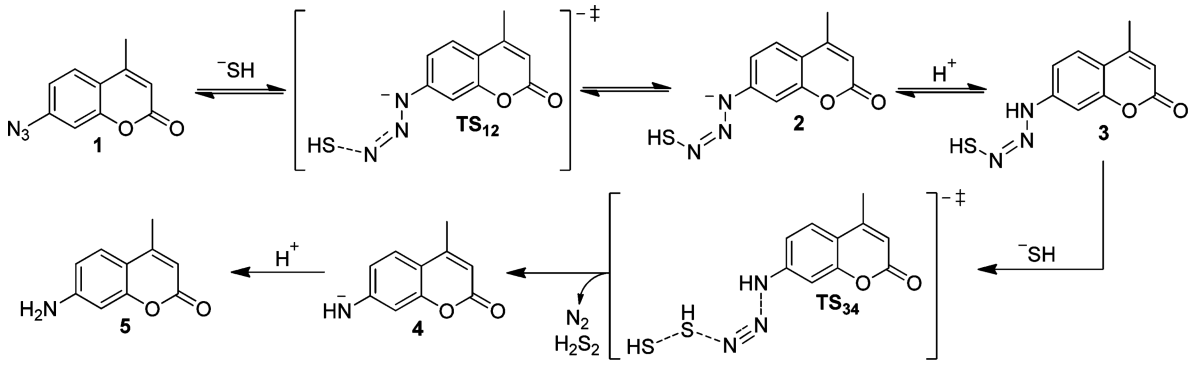

Scheme 2.

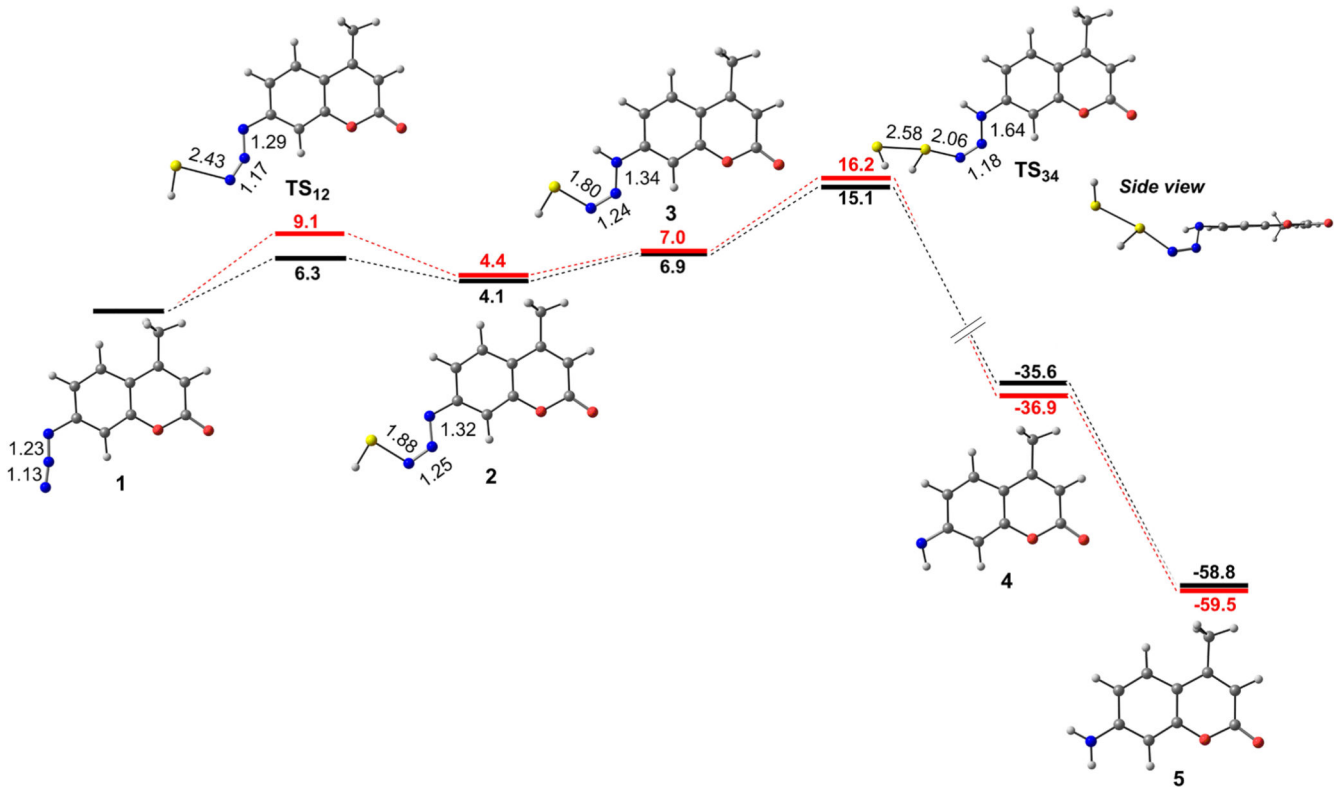

Figure 7.

Calculated potential energy surfaces for the proposed mechanism at the B3LYP/6-311++G(d,p) (black) and M06/def2-TZVPD (red) levels of theory with PCM solvation (H_2O). Energies are reported in kcal/mol.